Discovery of Potent Inhibitors of Dihydroneopterin Aldolase Using CrystaLEAD High-Throughput X-ray Crystallographic Screening and Structure-Directed Lead Optimization

William J. Sanders,* Vicki L. Nienaber, Claude G. Lerner, J. Owen McCall, Sean M. Merrick, Susan J. Swanson, John E. Harlan, Vincent S. Stoll, Geoffrey F. Stamper, Stephen F. Betz, Kevin R. Condroski, Robert P. Meadows, Jean M. Severin, Karl A. Walter, Peter Magdalinos, Clarissa G. Jakob, Rolf Wagner, and Bruce A. Beutel

Infectious Disease Research, Abbott Laboratories, 200 Abbott Park Road, Abbott Park, Illinois 60064-6217

Received October 3, 2003

Potent inhibitors of 7,8-dihydroneopterin aldolase (DHNA; EC 4.1.2.25) have been discovered using CrystaLEAD X-ray crystallographic high-throughput screening followed by structure-directed optimization. Screening of a 10 000 compound random library provided several low affinity leads and their corresponding X-ray crystal structures bound to the enzyme. The presence of a common structural feature in each of the leads suggested a strategy for the construction of a directed library of approximately 1000 compounds that were screened for inhibitory activity in a traditional enzyme assay. Several lead compounds with IC_{50} values of about 1 μM against DHNA were identified, and crystal structures of their enzyme-bound complexes were obtained by cocrystallization. Structure-directed optimization of one of the leads thus identified afforded potent inhibitors with submicromolar IC_{50} values.

Introduction

The increasing prevalence of microorganisms displaying resistance to known antibiotics has fueled continued interest in the discovery of potent, broad-spectrum antibacterial agents.[1] Among the most promising strategies for the development of new antibacterial therapeutics is the targeting of proteins essential for bacterial growth but lacking mammalian counterparts.[2] Characteristics of an ideal therapeutic target protein include broad conservation in the structure, or at least in the active site structure, across relevant bacterial strains. In addition, the lack of eukaryotic orthologues provides a greatly reduced chance of side effects induced by inhibition of similar proteins in humans.

The folate biosynthetic pathway has long been recognized as an attractive target for the development of selective antimicrobial agents.[3] Folate derivatives are essential cofactors in the synthesis of purines, pyrimidines, and amino acids in most organisms. Unlike humans and other mammals, bacteria are unable to absorb folate from their environment and must therefore synthesize it de novo. The biosynthetic pathway for the production of tetrahydrofolate (Figure 1) requires enzymes essential for bacterial growth, several of which do not possess eukaryotic orthologues.[4] A number of successful, marketed antibacterials including the sulfonamides (dihydropteroate synthase, DHPS)[5] and trimethoprim (dihydrofolate reductase, DHFR)[6] target enzymes in this pathway. DHPS and DHFR both possess the desired attributes of a successful antibacterial target: broad species homology and a lack of closely related enzymes in mammals. A third enzyme in the pathway, dihydroneopterin aldolase (DHNA; EC 4.1.2.25), catalyzes the retroaldol reaction of 7,8-dihydroneopterin (**3**) to afford glycoaldehyde and 6-hydroxymethyl-7,8-dihydropterin (**4**) (Figure 1).[4,7] Like DHPS and DHFR, DHNA is conserved across bacterial species and is nonexistent in humans. Unlike the former, however, DHNA has not been extensively investigated as a potential therapeutic target.[8]

X-ray Crystallography

The crystal structure of DHNA from *Staphylococcus aureus*, first reported by Hennig and co-workers,[9] shows that this enzyme crystallizes as an octamer of *I*422 symmetry. Specifically, the octamer is composed of two donut-shaped tetramers that come together to form a cylinder. The active site is located at the interface between monomer subunits of the tetramer such that one part of the active site is formed by one monomer while the other is formed by a second monomer, resulting in four active sites per tetramer (Figure 2). The crystal structure of DHNA in complex with the product of the enzyme-catalyzed reaction, 6-hydroxymethyl-7,8-dihydropterin **4** (Figure 3), was also reported by Hennig[9] and confirmed the location of the enzyme active site.

Many qualities of the reported DHNA crystal form make it a good candidate for lead discovery using high-throughput X-ray crystallographic screening.[10] The DHNA space group is high symmetry, thus requiring, on average, fewer data frames for a complete sampling of the unique section of the X-ray diffraction reciprocal lattice. This fact, coupled with the reported high-resolution diffraction of the crystals, suggests that data collection times should be relatively short on a high-intensity rotating anode source equipped with a detector with a short read-out time such as a charged-coupled device (CCD) detector.[11] Furthermore, because it was demonstrated that the ligand could be diffused into the

* To whom correspondence should be addressed. Phone: (847) 937-7168. Fax: (847) 935-5165. E-mail: will.sanders@abbott.com.

10.1021/jm030497y CCC: $27.50
Published on Web 02/18/2004

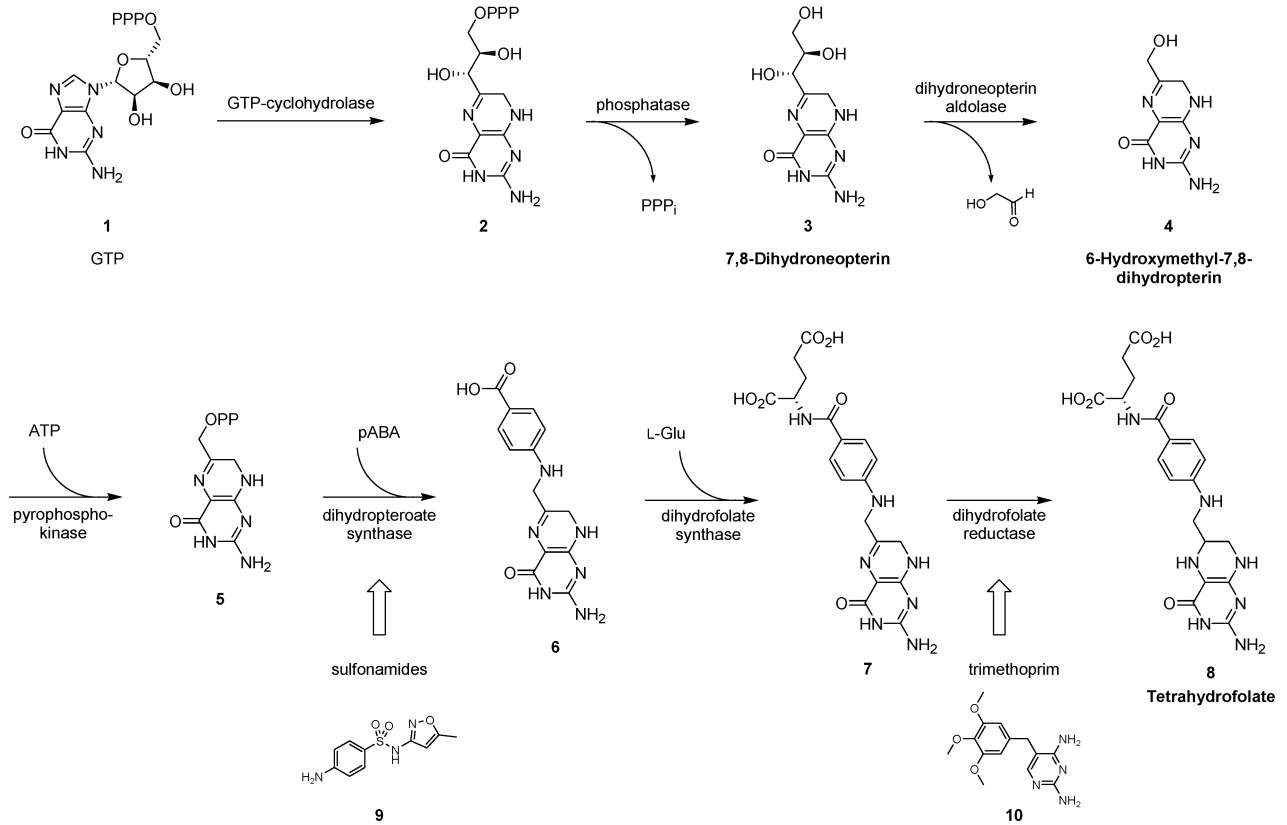

Figure 1. De novo biosynthesis of tetrahydrofolate. Enzymatic targets of marketed antibacterials sulfamethoxazole (**9**) and trimethoprim (**10**) are indicated with arrows.

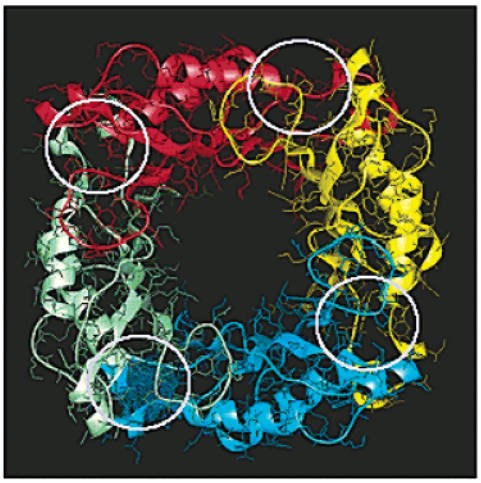

Figure 2. Ribbon diagram of dihydroneopterin aldolase showing the tetrameric structure with the four catalytic sites at monomer interfaces highlighted.

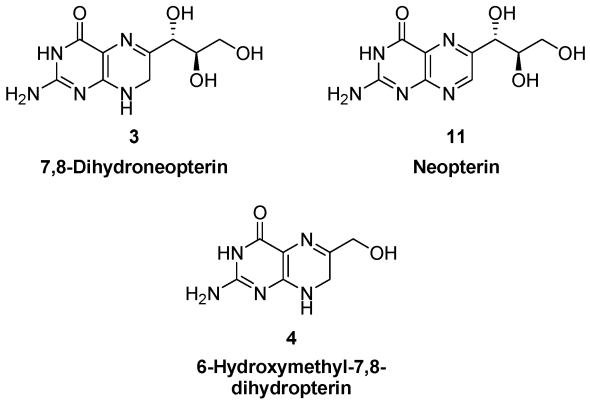

Figure 3. Structures of the DHNA native substrate 7,8-dihydroneopterin (**3**), substrate analogue neopterin (**11**), and the product of the enzyme-catalyzed reaction (**4**).

active site of intact DHNA crystals,[9] crystallographic screening for lead compound fragments (CrystaLEAD) was an ideal choice to screen for inhibitors of DHNA.[10] The combination of straightforward crystal production, a short acquisition time for diffraction data, and the ability to diffuse ligands into the active site of the intact crystal make DHNA a very attractive target for CrystaLEAD screening. A potential drawback to the use of crystallographic screening, however, is the location of the DHNA active site. Because the enzyme active sites are located at subunit interfaces within a tetramer, it is possible that the protein may undergo allosteric conformational transitions upon ligand binding that cannot occur in the crystalline state. An inability to make conformational transitions may cause crystal cracking upon treatment with ligand, resulting in crystals that do not diffract. Alternatively, diffraction-quality crystals with no ligand bound may result, leading to false negative binding data. However, because of our requirement for a lead compound and because published reports indicated that the natural substrate could be bound and that turnover could occur within the crystal lattice, crystallographic screening was performed with the possibility of false negative results taken into consideration.

The ability to diffuse ligands into an enzyme active site in its crystalline state is the preferred method for finding leads using the crystallographic screening method CrystaLEAD developed by Nienaber and co-workers.[10]

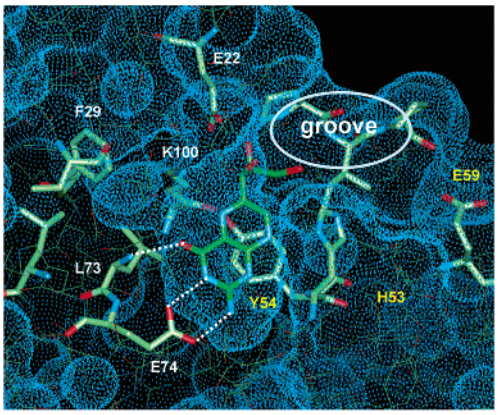

Figure 4. Model of neopterin bound in the active site of DHNA with key hydrogen bonds shown as dashed lines. The top right of the picture depicts an unoccupied groove that could be accessed to increase the potency of inhibitors.

Hence, although it was reported by Hennig and coworkers[9] that diffusion of ligands into DHNA crystals was successful, the uncleavable substrate analogue neopterin **11** (Figure 3) and the natural substrate 7,8-dihydroneopterin **3** (data not shown) were soaked into the crystals as positive controls. In both experiments, the diffused compound was clearly visible in the initial electron density maps ($2F_o - F_c$ contoured at 1σ and $F_o - F_c$ contoured at 2.5σ). As reported by Hennig, the bicyclic aromatic core of neopterin is highly ordered, while the terminus of the aliphatic triol substituent becomes disordered in the electron density map. Examination of the neopterin/DHNA complex structure shows a binding mode for the inhibitor that is similar to the product complex previously reported.[9] Notably, there appear to be three polar groups on the inhibitor that are engaged in hydrogen bonds with the protein at the monomer−monomer interface (Figure 4). This gives rise to a three-point hydrogen-bonding motif between the inhibitor and the protein that is probably critical for substrate recognition. Specifically, hydrogen bonds exist between the 4-carbonyl of the ligand and the backbone nitrogen of Leu 73 of one of the monomers (molecule A) as well as between the 3-position −NH of the inhibitor and Glu 74-Oδ1 of molecule A. The exocyclic 2-amino group of the ligand is donating hydrogen bonds to Glu 74-Oδ2 of molecule A and to Val 52-O of the second protein monomer (molecule B, not shown). The ordered solvent molecule reported in the literature structure[9] that is hydrogen-bonding with Asn 71-O, Lys 100-Nζ (both in molecule A), and the 4-carbonyl of the inhibitor is also observed in the neopterin complex structure. Interestingly, the substrate binding pocket shows some similarity to the primary binding pocket of trypsin-like proteases.[12] Glu 74, which is located at the base of the DHNA pocket, is analogous to Asp 189 of the trypsin-like proteases. This similarity suggests that screening of directed libraries designed to identify inhibitors of trypsin-like enzymes could be a source of lead compounds for DHNA as well. Upon completion of exploratory experiments and evaluation of the DHNA active site structure, crystallographic screening for lead compounds was initiated.

A 10 000 compound library was divided into 100-compound sublibraries with sufficient structural diversity to allow for direct hit identification from the electron density map of a bound complex. The sublibraries were then screened as mixtures, resulting in the identification of two ligands bound to DHNA (parts A and B of Figure 5). Both compounds occurred in the same 100-compound sublibrary and were unambiguously identified from the mixture without deconvolution based on the shape of the initial electron density maps.[10] Both hits shared the three-point hydrogen-bonding motif of the substrate analogue depicted in Figure 4 and were subsequently shown to be competitive inhibitors of DHNA. 9-Methylguanine **12** (Figure 5A) was found to inhibit DHNA in the enzymatic assay with an IC_{50} of 28 μM. Compound **13**, a 2-aminopyrimidine (Figure 5B), similarly inhibited the enzyme but was less potent with an IC_{50} of 80 μM. Because of the similarity between the DHNA binding pocket and the primary binding site (S1) of trypsin-like serine proteases mentioned above, a fragment library designed to be screened against the trypsin-like protease urokinase[10] was also screened for DHNA binders. This screen resulted in identification of compound **14**, an 8-aminopurine analogue (Figure 5C). Because the 8-aminopurine analogue is symmetric, the molecule can be fitted into the electron density in two possible orientations. The orientation shown in Figure 5C is the conformation in which the inhibitor maintains a hydrogen bond with Leu 73-N as in the substrate/enzyme complex. Compound **14** was also

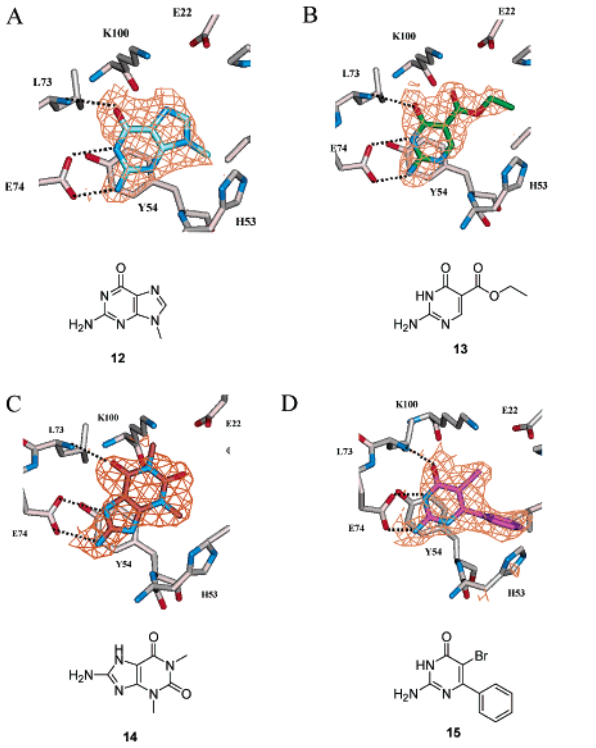

Figure 5. Results of crystallographic screening experiments. All maps shown are the initial $2F_o - F_c$ maps calculated for the protein in the absence of inhibitor. These are the maps that were examined for analysis of the crystallographic screening data: (A) 9-methylguanine (**12**, IC_{50} = 28 μM) at 2.2 Å resolution; (B) 2-amino-4-hydroxy-5-carboxyethylpyrimidine (**13**, IC_{50} = 80 μM) at 2.2 Å resolution; (C) 8-amino-1,3-dimethyl-3,7-dihydropurine-2,6-dione (**14**, IC_{50} = 50 μM) at 2.3 Å resolution; (D) 2-amino-5-bromo-3-hydroxy-6-phenylpyrimidine (**15**, IC_{50} = 38 μM) at 2.1 Å resolution. Hydrogen bonds between each inhibitor and DHNA are depicted by dashed lines.

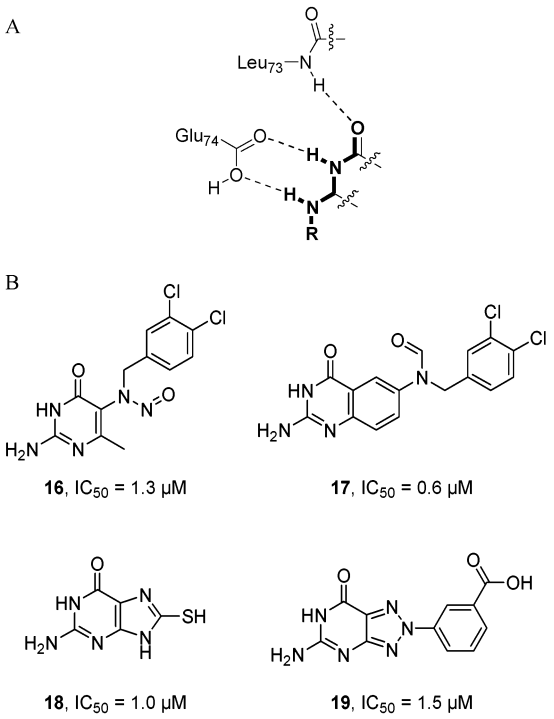

Figure 6. (A) Three-point hydrogen-bonding motif used in the construction of a directed library for enzyme inhibition screening. (B) Inhibitors identified in an enzyme inhibition assay of a directed library.

shown to be a competitive inhibitor of DHNA with an IC_{50} of 50 μM. Finally, a third library consisting solely of aminopyrimidines was screened, resulting in a fourth hit. Compound **15** (Figure 5D) was identified from its X-ray diffraction pattern and was shown to competitively inhibit DHNA with an IC_{50} of 38 μM.

Of the four lead scaffolds identified from the crystallographic screens, three (**12**, **13**, and **15**) contained the exact three-point hydrogen-bonding motif present in the substrate analogue neopterin and in the bound product 6-hydroxymethyl-7,8-dihydropterin, and the fourth (**14**) displayed hydrogen bonds to the same protein residues but with different atom connectivity in the ligand. As mentioned above, it was recognized early that false negative binding data may result if an allosteric conformational shift occurred in the enzyme active site upon ligand binding. The presence of an identical hydrogen-bonding motif in three of the four CrystaLEAD hits and in both the substrate analogue and the enzyme-catalyzed reaction product suggested that screening of a much smaller, directed library in an enzymatic assay might prove to be fruitful. To this end, a library consisting of ~1000 compounds all containing the $H_2N-C-NH-C=O$ substructure (Figure 6A) was constructed. Screening of this directed library in the enzymatic assay provided several hits with IC_{50} values on the order of 1 μM (Figure 6B) as well as a larger number with IC_{50} values from 10 to 50 μM (structures not shown).

Although the leads identified in the secondary screen proved to be more potent than the original compounds identified by CrystaLEAD, it was not possible to obtain crystal structures by the compound soaking method. Interestingly, all of these compounds displayed sigmoidal inhibition curves in the enzyme assay (Figure 7), consistent with cooperativity in the enzymatic assay and

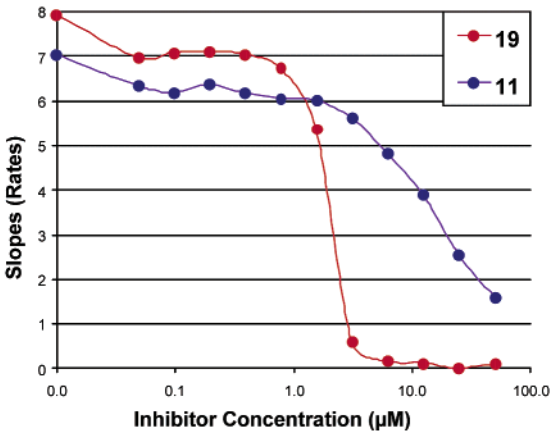

Figure 7. Representative enzyme inhibition curves. The rate of the enzymatic reaction is plotted vs increasing inhibitor concentration, and IC_{50} is determined by the concentration of compound that causes a 50% decrease in the initial reaction rate. The curve observed for **11** is typical of weak inhibitors, while the curve observed for **19** shows a much steeper slope, typical of more potent inhibitors.

indicating a possible conformational shift during ligand binding. Examples of the two types of inhibition curves observed for DHNA inhibitors are illustrated in Figure 7. The moderately sloped curve of weak inhibitors is represented by neopterin **11**, while the steeply sloped curve of carboxylic acid **19** is representative of more potent inhibitors. Since a conformational shift during ligand binding was suspected, individual cocrystallization experiments were performed in the presence of a number of the lead compounds identified in the directed library screen. Almost all of the compounds were successfully cocrystallized, yielding isomorphous crystals (space group *I*422) similar to the crystals obtained by the crystal soak method. One compound, however, afforded crystals in which a space group shift to *P*4(2)-22 with a dimer rather than a monomer in the asymmetric unit occurred. Still, close visual comparison of each monomer of this dimer to the *I*422 monomer showed no significant difference in the crystal lattices. These results suggest that a conformational shift that cannot occur in the crystal lattice does transpire during compound binding; however, the final bound structure remains quite similar to the apo structure. These data also suggest that binding outside the primary binding site and into an extended groove illustrated in Figure 4 could trigger this shift. Hence, it is possible that compounds present in the original 10 000 compound library could require a similar conformational shift and would therefore not bind to the crystalline state of DHNA. Although the possibility exists that potential leads were overlooked because of the inability of the crystal soaking method to identify compounds in which a conformational transition occurs upon binding, the variety and potency of those hits identified were sufficient to provide promising leads for structure-based optimization.

Design, Synthesis, and Activity of Inhibitors

In the crystal structure of the neopterin/DHNA complex, the neopterin heterocylic ring occupies most of the volume of the DHNA substrate binding pocket. Since this orientation proved to be identical for all of

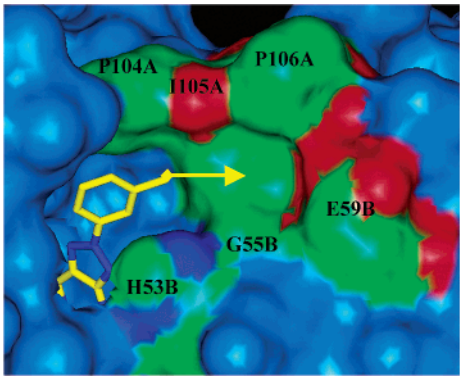

Figure 8. Molecular model of lead compound **19** bound to DHNA constructed from the X-ray crystal structure of the bound complex showing potential for access to an extended binding groove. The protein surface is shown in blue with the amino acids lining the groove (104−106 molecule A; 53, 55, and 59 molecule B) highlighted in green and red. The binding mode of the inhibitor is shown in yellow.

the lead molecules identified, additional nearby sites were sought for exploitation in structure-based design cycles to engineer both potency and specificity into inhibitors. An examination of the active site and the surrounding area identified an extended binding groove above the heterocyclic ring, which could theoretically be occupied by substitution of a ligand bound in the primary binding pocket (Figure 4). This site is lined by Pro 104, Ile 105, and Pro 106 of one monomer subunit and by His 53, Gly 55, and Glu 59 of a second monomer subunit and is partially occupied by the aliphatic triol of neopterin in the substrate analogue complex. Hence, a potential design strategy would be to access this extended binding groove by chemical extension of a lead bound in the primary pocket. The ideal lead compound for DHNA would have a binding orientation that would facilitate access to this extended binding site through additional chemical elaboration. Of the four most potent compounds discovered in the secondary enzymatic assay, carboxylic acid **19** appeared to be the most promising both in terms of its bound orientation and in its obvious prearrangement for chemical modification. Figure 8 shows a surface area model of the DHNA active site occupied by compound **19** (oxygen atoms of the carboxylic acid moiety are not shown) constructed from the X-ray structure of the bound complex. From the structure, it is clear that the carbon atom of the carboxylic acid group is pointing directly into the unoccupied groove described above. The trajectory of the carboxylic acid carbon is such that substitution with functionality designed to fill the unoccupied groove should afford new contacts with the enzyme and thus increased potency of inhibitors.

Synthetic opportunities for the functionalization of a carboxylic acid moiety abound. Through simple, well-precedented chemistry, carboxylic acid **19** could be easily converted into a library of amides, esters, amines, or ethers as well as a wide variety of more complex functional groups. In this case, since the initial objective was to discover space-filling groups to enhance the potency of inhibitors, the carboxylic acid was viewed simply as a linker to which to append a variety of space-filling substituents. Because of the simplicity of amide bond formation and the wide variety of commercially

Scheme 1[a]

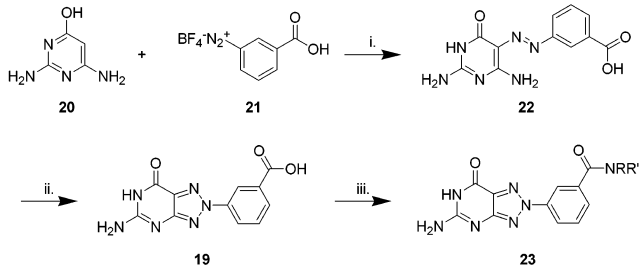

[a] Reagents and conditions: (i) 1.4 M NaOAc, 91%; (ii) $CuSO_4$, pyridine, H_2O, reflux, 85%; (iii) RR′NH, EDC, DIPEA, DMF.

Table 1. Side Chain Structures and Inhibitory Potencies of Benzylic Amide Derivatives of Lead Compound **19**

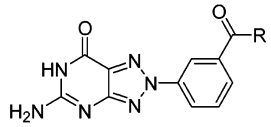

Compound	R	IC_{50} (μM)
19		1.5
24	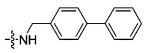	25
25	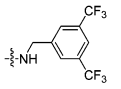	1.0
26	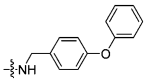	22
27	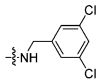	0.068
28	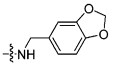	0.31
29	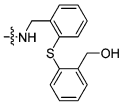	0.30
30	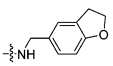	0.55

available amines, amides of **19** were chosen as the initial target compounds. Scheme 1 illustrates the synthetic approach to these molecules. Carboxylic acid **19** was synthesized as previously reported,[13] with slight modifications. 2,6-Diamino-4-hydroxypyrimidine **20** was treated with 3-carboxybenzenediazonium tetrafluoroborate **21**[14] in aqueous sodium acetate to afford the diazine **22** in 91% yield. Oxidative cyclization of **22** in the presence of copper(II) sulfate afforded **19** in 85% yield. Standard carbodiimide-promoted amide formation then afforded the target compounds in good yield and high purity.

Tables 1 and 2 depict a sampling of the compounds synthesized by this method and their inhibitory activities against DHNA. The initial set of derivatives prepared included a variety of benzylamides (Table 1) and hydroxyalkylamides (Table 2) designed simply to test the possibility of increasing inhibitor potency by filling the open area surrounding the primary binding pocket. A combination of hydrophobic and hydrophilic substituents was included to maximize the chances for in-

Table 2. Side Chain Structures and Inhibitory Potencies of Hydroxyalkyl Amide Derivatives of Lead Compound **19**

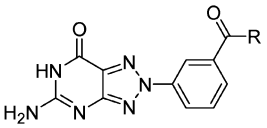

Compound	R	IC_{50} (μM)
19		1.5
31		2.3
32	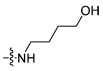	2.0
33		0.95
34		0.73
35		0.74
36		0.41
37		0.32
38		0.35

creased potency through new ligand−enzyme interactions. Although the native substrate and the product of the enzyme-catalyzed reaction both contain hydroxyl groups, the nature of the extended binding groove is primarily hydrophobic, suggesting that hydrophobic substituents would provide the largest potency boost. Additionally, both small and large substituents were included because of evidence of conformational transformation upon binding. The possibility of a change in the position of active site residues such as His 53, which was observed in the X-ray structures of several related compounds (data not shown) resulting in significant enlargement of the binding pocket, required the inclusion of amide substituents that qualitatively appeared too large to fit into the cavity.

As expected and as the data in Tables 1 and 2 illustrate, the potency of inhibitors is increased by filling the open space in the extended groove protruding from the active site. The most potent compound prepared in the current study is 3,5-dichlorobenzyl amide **27** with an IC_{50} of 68 nM. Figure 9 shows the inhibition curve of **27** along with that of the lead compound **19**. As described above, the curve is sigmoidal in shape, indicating a possible conformational transition upon binding. The variety of sizes and shapes of side chain substituents investigated here provides a limited picture of the nature of the newly identified binding site. The variation of IC_{50} values among similarly substituted compounds suggests a strong SAR within the binding site; however, a much larger set of analogues is required to more thoroughly probe the nature of this SAR. Of particular interest are compounds **25** and **27** (Table 1). Compound **27**, the most potent inhibitor of DHNA

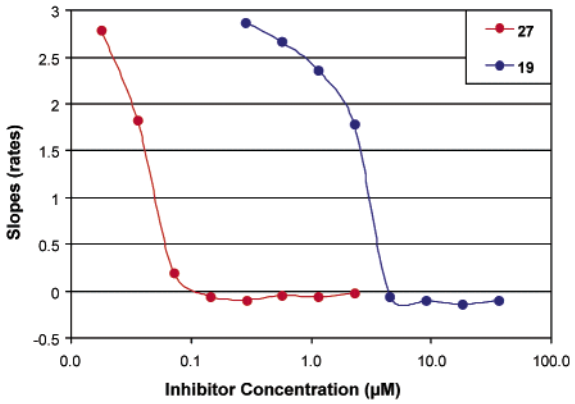

Figure 9. Enzyme inhibition curves for lead compound **19** and for compound **27**, the most potent inhibitor identified.

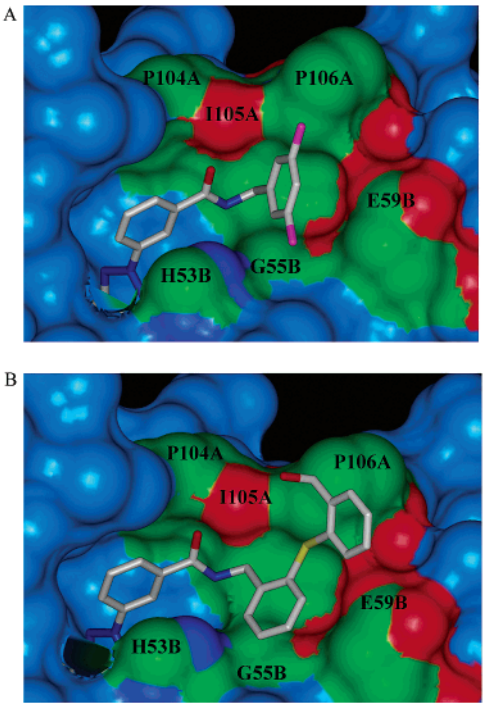

Figure 10. Molecular models of compounds **27** and **29** bound to DHNA constructed from the X-ray crystal structures showing occupation of the extended binding groove by aromatic rings.

reported here, displays an IC_{50} that is 20-fold more potent than the initial lead. The substitution of two trifluoromethyl moieties for two chlorine atoms affords compound **25**, which is 15 times less potent than **27**. The observation of a large difference in potency between two compounds of such similar size and shape indicates that further optimization is quite feasible. Another compound with promising indications for further optimization is biphenyl thioether **29**. Although not as potent as **27**, compound **29** is 3-fold more potent than the lead. More importantly, the X-ray structure of **29** illustrates additional potential for structure-directed optimization. X-ray structures of **27** and **29** are shown in Figure 10 and illustrate a key feature of the initial SAR. The biphenyl thioether substituent was chosen because it qualitatively appeared too large to fit into the binding site. However, the IC_{50} was surprisingly potent, the reason for which is illustrated in the crystal structure. In contrast to compound **27** (Figure 10A), the

conformation of **29** (Figure 10B) has shifted slightly in the active site. While the core of the molecule remains fixed, a slight rotation about the C(O)N−C bond pushes the first phenyl ring lower and allows space for the second phenyl ring to fit. The ability of the binding site to adapt to conformational variation among ligands combined with evidence of a strong SAR provides a solid foundation for the identification of even more potent inhibitors of DHNA.

Although one of the goals of this work was to identify potent in vitro inhibitors of DHNA, the ultimate objective is the development of new antibacterial chemotherapies. While structure-directed lead optimization led to the synthesis of numerous compounds with IC_{50} values less than 1 μM, including one with an IC_{50} of 68 nM, none of the compounds prepared here inhibited the growth of bacteria including *Staphylococcus aureus*, *Streptococcus pneumoniae*, *Moraxella catarrhalis*, *Haemophilus influenzae*, *Enterococcus faecium*, *Streptococcus pyogenes*, and *Staphylococcus epidermidis*. In addition, the compounds were not active against a hypersusceptible *Escherichia coli* permeability mutant and Acr^- efflux pump mutants of H. *influenzae* and E. *coli*. The compounds were also inactive in the presence of permeability-enhancing agents including EDTA, nisin, polymyxin B nanopeptide, and the efflux pump inhibitor reserpine. Finally, none of the compounds described here demonstrated the ability to inhibit bacterial uptake of radiolabeled *p*-aminobenzoic acid, a key indicator to the inhibition of folate biosynthesis.[15] The surprising lack of even weak antibacterial activity in multiple assays including those performed in the presence of cell-permeablizing agents and efflux inhibitors could have several explanations. The use of permeablizers would seem to rule out poor cell penetration as an issue, so it is possible that inactivation of the inhibitors by intracellular enzymes could be occurring or that nonspecific binding to intracellular proteins or the cell membrane may reduce the available inhibitor concentration. An alternative and much more intriguing possibility is that the intracellular concentration of the DHNA substrate 7,8-dihydroneopterin could be quite high relative to the K_m of the enzyme. In this case, even compounds with submicromolar inhibitory activity are not potent enough to decrease the intracellular folate pools to growth-inhibitory levels. (It has been shown that upon treatment with trimethoprim, intracellular folate pools drop to 25% of uninhibited levels within 4 h.[16]) In any case, we can conclude that although the current compounds are potent inhibitors of DHNA in vitro, they do not show promise as antibacterial therapeutics.

Conclusion

We have reported an example of high-throughput X-ray crystallographic screening for an apparently allosteric enzyme. These data seem to show that a conformational shift that is not achievable in the crystalline state of the enzyme is required for the binding of potent inhibitors to DHNA, although the bound and unbound enzyme conformations are identical. While X-ray crystallographic screening of random libraries afforded inhibitors with weak IC_{50} values in the range 20−80 μM, a traditional enzyme screen of a directed library afforded much more potent inhibitors with X-ray structures obtainable only by cocrystallization. This result clearly illustrates a potential problem with crystallographic screening and structure-directed drug design in general. While the crystalline state of an enzyme may select primarily for favorable conformations among compounds within a screening library, the soluble enzyme can have entirely different requirements. In the case of DHNA, a large, extended binding site that is not accessible within the crystalline state of the enzyme becomes accessible through conformational flexibility in the soluble enzyme. We have shown that a significant improvement in IC_{50} values could be realized by filling this extended binding site through structure-directed design and anticipate further improvement with repeated design cycles.

Experimental Section

Enzyme Preparations. The double-stranded DNA encoding DHNA was isolated by PCR amplification from *Staphylococcus aureus* genomic DNA using oligodeoxynucleotide primers (5′-GGAATTCACATATGCAAGACACAATCTTTCTTAAAGG and 5′-GCGACGTACTCGAGTTATTTATTCTCCCTCACTATTTCGATAC) based on the DHNA gene sequence (preliminary sequence data were obtained from The Institute for Genomic Research website at http://www.tigr.org). The gene was cloned into the NdeI-XhoI restriction sites of the expression vector pET-30b (Novagen, Madison, WI) behind the T7lac promoter. A TAA-stop codon was inserted between the last codon of the protein and any vector-derived C-terminal tail so that only the native protein sequence was translated. All vector sequences were confirmed by bidirectional dye-terminator DNA sequencing. The resulting construct was transformed into *Escherichia coli* BL21(DE3) for expression. Large-scale expressions (17 L culture volume) were carried out in a New Brunswick Scientific (Edison, NJ) Micros fermentor. Cells were grown in SBG medium [per liter: 60 g of Superbroth (Q-Biogene, Carlsbad, CA), 10 mL of 1% DF-60 antifoam, 10 mL of 30% glucose, 1 mL of trace element solution]. The fermentations were carried out at 30 °C, and the pH was maintained at 7.00 through automatic addition of the appropriate pH titrants (4 N KOH/4 N H_2SO_4). Air was sparged at a constant rate of 2 vvm (vvm = liters of air per liter of medium per minute), and the dissolved oxygen concentration was maintained at or above 45% air saturation throughout the entire run via a cascaded control loop that automatically adjusted the agitation rate as needed. A 30% glucose solution was fed during a portion of the ferment to maintain the glucose concentration between 0.1 and 2 g/L. When the cultures reached an optical density (OD) of 3.7, protein expression was induced by addition of 1 mM IPTG. Cells were harvested 4 h postinduction with a resulting cell yield of ∼27 g wet wt/L. The protein was expressed well and was ∼80% soluble.

DHNA was purified by a modification of the procedure of Hennig et al.[9] Briefly, 20 g of cells were resuspended in buffer A (25 mM Tris, pH 8.0 at 4 °C, 50 mM NaCl, 5% glycerol, 2 mM EDTA, 1 mM PMSF, 1 mM NaN_3) and disrupted using a French press. Following centrifugation, the supernatant was loaded onto a 5 cm × 31 cm DEAE-Sepharose FF column (Amersham Pharmacia Biotech, Picataway, NJ). The protein was eluted with a linear gradient of 0−1 M NaCl in buffer A. The fractions containing the DHNA were pooled and dialyzed into buffer A. The dialyzed pool was then loaded on a 2.6 cm × 38 cm Q-Sepharose FF column (Amerscham Pharmamcia Biotech, Picataway, NJ) and eluted with a linear gradient of 0−1 M NaCl in buffer A. The fractions containing the DHNA were pooled and concentrated and then applied to a 2.6 cm × 60 cm Sephacryl S300 HR column (Amerscham Pharmamcia Biotech, Piscataway, NJ) equilibrated in 25 mM Tris, 5% glycerol, 50 mM NaCl, and 1 mM NaN_3 (buffer B). The purified DHNA was pooled and filter-sterilized. Recovery averaged about 6 mg of purified protein per gram of cell paste.

Material thus purified routinely crystallized, with the resulting crystals defracting to better than 2.5 Å.

X-ray Crystallography. Crystals were obtained using published conditions.[9] As reported, the protein was found to crystallize under a number of different conditions using the commercially available Crystal Screen 1 (Hampton Research, Laguna Niguel, CA) and was found to diffract to high resolution (1.6−2.0 Å). In this study, crystals from condition no. 26 (0.2 M ammonium acetate, 0.1 M trisodium citrate, pH 5.6, 30% MPD) were used for this series of experiments because the mother liquor was found to be cryoprotectant. Crystallographic data were processed, and structures were determined and refined by standard methods using the program packages DENZO,[17] CNX, and QUANTA. Crystallographic screening data were acquired using a Rigaku rotating anode generator equipped with Osmic mirrors and a MarCCD detector. All screening data were collected using a robotic crystal mounting and alignment robot[18] with data collection times of 2 h per crystal. To facilitate rapid data collection, crystals were visually prealigned in the mounting loops such that data would be sampled along the crystallographic 4-fold axis. DHNA was screened against a fragment library consisting of 10 000 compounds divided into 100 compound shape-diverse mixtures. It was possible to achieve shape diversity for each mixture because the relatively small compound library was designed for maximum overall diversity to increase the likelihood of finding lead compounds for a varied assortment of enzyme active sites. The library and shape diverse mixtures were generated computationally.[10] The 10 000 compounds were primarily obtained from the Abbott chemical repository, although some were identified in the Available Chemicals Directory (ACD) and purchased commercially.

Enzyme Inhibition Assay. Inhibition of DHNA activity was quantified using a fluorescence-based kinetic enzyme assay monitoring formation of the reaction product 6-hydroxymethyl-7,8-dihydropterin.[19] The assay was performed in a 96-well microtiter plate format using a Perkin-Elmer HTS 7000 Plus bioassay reader set for an excitation wavelength of 430 nm and an emission wavelength of 535 nm. Each reaction was monitored for 1 h with the mean reaction rate integrated over this time. The rate remained essentially linear throughout this period when using the reaction parameters specified. Each reaction was in a total volume of 150 μL in buffer consisting of 20 mM HEPES (pH 7.4) and 150 mM NaCl. DHNA was present at 50 nM concentration and showed no decrease in activity following dilution or prolonged incubation. The substrate 7,8-dihydroneopterin (Fluka, Alexis) was present at an initial concentration of 4 μM. Reactions were run at ambient temperature with the internal temperature of the plate reader at approximately 29 °C.

Synthetic Materials and Methods. Unless otherwise specified, reactions were performed in oven-dried glassware under an inert atmosphere of nitrogen and monitored by thin-layer chromatography (TLC) or by liquid chromatography−mass spectrometry (LC−MS). All reagents were purchased from commercial suppliers and used as provided. Analytical TLC was performed on 0.25 mm precoated Merck silica gel 60 F_{254}, visualizing with ultraviolet light at 254, 302, or 365 nm wavelength. Flash column chromatography was performed on a Biotage Flash 40 system using 50 or 90 g of prepacked silica columns and HPLC grade solvents. Analytical LC−MS was performed on an Agilent series 1100 HPLC system equipped with an autosampler and coupled to a Finnegan Thermoquest atmospheric pressure chemical ionization (APCI) mass spectrometer. Peak detection was by ultraviolet absorption at 220 and 254 nm and by an evaporative light scattering detector (ELSD). Proton nuclear magnetic resonance (^{1}H NMR) spectra were recorded on a Bruker ARX spectrometer (300 MHz) or on a Varian Inova spectrometer (500 MHz) and are referenced to residual solvent peaks (DMSO-d_6, δ 2.50 ppm) or to an internal standard of tetramethylsilane (TMS, δ 0.00 ppm). ^{1}H−^{1}H couplings are assumed to be first-order, and peak multiplicity is reported as s (singlet), d (doublet), t (triplet), q (quartet), m (multiplet), and b (broad). Electrospray ionization (ESI) and desorption chemical ionization (DCI) mass spectrometry were performed on Finnigan SSQ700 single quadrupole mass spectrometers. Elemental analyses were performed by Robertson Microlit Laboratories (Madison, NJ). All of the compounds reported below were analyzed by LC−MS, ^{1}H NMR, and mass spectrometry and are consistent with the proposed structures in each case. Analytical purity was assessed by reverse-phase HPLC on a Phenomenex Luna C8 column (5 μM, 2.0 mm × 30 mm, 5 μL injection volume) using a solvent gradient of 10−100% acetonitrile in 0.1% aqueous trifluoroacetic acid over 4 min at a flow rate of 1.5 mL/min and detecting by UV absorption at 220 and 254 nm and by ELSD.

3-Carboxybenzenediazonium Tetrafluoroborate (21).[14] 3-Aminobenzoic acid (10.0 g, 72.9 mmol) was dissolved in 182 mL of ethanol and tetrafluoroboric acid (28.6 mL, 219 mmol) was added, resulting in a clear solution with a small amount of undissolved material. The mixture was cooled to 0 °C, and isoamyl nitrite (29.4 mL, 219 mmol) was added dropwise. After the mixture was stirred at 0 °C for 20 min, a precipitate formed. Diethyl ether was added, and stirring continued for 30 min. The precipitate was filtered, rinsed thoroughly with diethyl ether, and dried under vacuum. A total of 16.6 g (97%) of white crystals was isolated. ^{1}H NMR (300 MHz, DMSO-d_6) δ ppm 8.10 (t, J = 7.8 Hz, 1H), 8.68 (ddd, J = 8.2, 1.4, 1.1 Hz, 1H), 8.85 (ddd, J = 8.2, 2.1, 1.1 Hz, 1H), 9.23 (t, J = 1.7 Hz, 1H).

3-(2,4-Diamino-6-hydroxy-4,5-dihydropyrimidin-5-yl-azo)benzoic Acid (22).[13] 2,4-Diamino-6-hydroxypyrimidine (8.35 g, 66.2 mmol) was dissolved in 500 mL of 1.4 M sodium acetate, followed by slow addition of 3-carboxybenzenediazonium tetrafluoroborate (16.4 g, 69.5 mmol). A thick, orange precipitate quickly formed, and the mixture was stirred at room temperature overnight. The precipitate was filtered, rinsed with water, ethanol, and diethyl ether, and dried under vacuum to afford 22.0 g (100%) of an orange solid consistent with the trihydrate. ^{1}H NMR (300 MHz, DMSO-d_6) δ ppm 7.22 (br s, 2H), 7.48 (t, J = 7.6 Hz, 1H), 7.79 (m, 2H), 7.92 (d, J = 3.7 Hz, 1H), 8.15 (s, 1H), 10.32 (br s, 1H), 11.08 (br s, 1H). MS [(−)-ESI] m/z 273 [M − H]$^-$.

3-(5-Amino-7-hydroxy-[1,2,3]triazolo[4,5-*d*]pyrimidin-2-yl)benzoic Acid (19). Copper(II) sulfate (2.19 g, 13.7 mmol) was dissolved in 30 mL of 1:1 water/pyridine, and the resulting mixture was heated to reflux. Compound **22** (1.50 g, 4.57 mmol) was carefully added to the hot solution, causing the reaction mixture to turn dark-green. After the mixture was refluxed overnight, a light-blue suspension formed, which was cooled to room temperature and poured into water. A precipitate formed, which was filtered and rinsed with water and 5% acetic acid. A green solid was isolated, which was dissolved in 5% sodium hydroxide and filtered. The yellow filtrate was stirred over activated charcoal, filtered, and acidified with 1 M hydrochloric acid. A gelatinous precipitate formed, which was filtered and rinsed thoroughly with water, followed by ethanol and diethyl ether. A very light-green solid was isolated, which was dried under vacuum to afford 1.24 g (100%) of the title compound. ^{1}H NMR (300 MHz, DMSO-d_6) δ ppm 6.75 (br s, 2H), 7.74 (t, J = 8.1 Hz, 1H), 8.02 (ddd, J = 7.9, 1.1, 1.0 Hz, 1H), 8.32 (ddd, J = 8.1, 2.4, 1.0 Hz, 1H), 8.59 (t, J = 2.0 Hz, 1H), 11.18 (s, 1H), 13.38 (br s, 1H). MS [(−)-ESI] m/z 271 [M − H]$^-$.

General Procedure for Amide Synthesis. Compounds **24**−**38** were synthesized in a LabTech Platform IV parallel synthesizer from Advanced ChemTech using a 40-well solution-phase reaction block. In each well, compound **19** (0.200 g, 0.735 mmol), an appropriate amine (1.5 equiv, 1.10 mmol), 1-(3-dimethylaminopropyl)-3-ethylcarbodiimide hydrochloride (0.155 g, 0.808 mmol), 1-hydroxybenzotriazole hydrate (0.124 g, 0.808 mmol), and *N*,*N*-diisopropylethylamine (0.384 mL, 2.20 mmol) were combined in 3.7 mL of anhydrous, amine-free *N*,*N*-dimethylformamide, and the mixtures were shaken at 350 rpm at room temperature overnight. The reaction mixtures were diluted with water and filtered, and the resulting solids were rinsed sequentially with 1 M hydrochloric acid, 5% sodium hydroxide, water, ethanol, and diethyl ether.

Each compound was isolated as an off-white powder requiring no further purification.

3-(5-Amino-7-hydroxy-[1,2,3]triazolo[4,5-*d*]pyrimidin-2-yl)-*N*-biphenyl-4-ylmethylbenzamide (24): ^{1}H NMR (300 MHz, DMSO-d_6) δ ppm 4.56 (d, J = 5.8 Hz, 2H), 6.71 (br s, 2H), 7.35 (m, 1H), 7.41−7.49 (m, 4H), 7.60−7.66 (m, 4H), 7.72 (t, J = 8.1 Hz, 1H), 8.02 (ddd, J = 8.0, 1.4, 1.2 Hz, 1H), 8.25 (ddd, J = 8.1, 2.4, 1.0 Hz, 1H), 8.63 (t, J = 1.7 Hz, 1H), 9.40 (t, J = 5.9 Hz, 1H), 11.11 (s, 1H). MS [(−)-ESI] m/z 496 [M + CH_3CO_2]$^-$. Anal. ($C_{24}H_{19}N_7O_2$) C, H, N.

3-(5-Amino-7-hydroxy-[1,2,3]triazolo[4,5-*d*]pyrimidin-2-yl)-*N*-(3,5-bistrifluoromethylbenzyl)benzamide (25): ^{1}H NMR (300 MHz, DMSO-d_6) δ ppm 4.70 (d, J = 5.8 Hz, 2H), 6.36 (br s, 2H), 7.68 (t, J = 8.0 Hz, 1H), 7.92 (d, J = 8.1 Hz, 1H), 8.01 (s, 1H), 8.06 (s, 2H), 8.23 (ddd, J = 8.1, 2.0, 0.68 Hz, 1H), 8.59 (s, 1H), 9.48 (t, J = 5.8 Hz, 1H). MS [(−)-ESI] m/z 496 [M − H]$^-$.

3-(5-Amino-7-hydroxy-[1,2,3]triazolo[4,5-*d*]pyrimidin-2-yl)-*N*-(4-phenoxybenzyl)benzamide (26): ^{1}H NMR (300 MHz, DMSO-d_6) δ ppm 4.50 (d, J = 5.9 Hz, 2H), 6.74 (br s, 2H), 6.99 (m, 4H), 7.12 (t, J = 7.4 Hz, 1H), 7.38 (m, 4H), 7.70 (t, J = 7.9 Hz, 1H), 8.00 (d, J = 8.1 Hz, 1H), 8.24 (dt, J = 8.1, 1.1 Hz, 1H), 8.61 (t, J = 1.7 Hz, 1H), 9.37 (t, J = 5.9 Hz, 1H), 11.20 (br s, 1H). MS [(−)-ESI] m/z 452 [M − H]$^-$. Anal. ($C_{24}H_{19}N_7O_3\cdot H_2O$) C, H, N.

3-(5-Amino-7-hydroxy-[1,2,3]triazolo[4,5-*d*]pyrimidin-2-yl)-*N*-(3,5-dichlorobenzyl)benzamide (27): ^{1}H NMR (300 MHz, DMSO-d_6) δ ppm 4.52 (d, J = 5.9 Hz, 1H), 6.73 (br s, 2H), 7.40 (d, J = 1.8 Hz, 2H), 7.51 (t, J = 1.8 Hz, 1H), 7.72 (t, J = 8.1 Hz, 1H), 8.01 (dt, J = 8.1, 1.5 Hz, 1H), 8.26 (ddd, J = 8.1, 2.2, 1.1 Hz, 1H), 8.61 (t, J = 1.8 Hz, 1H), 9.42 (t, J = 5.9 Hz, 1H), 11.11 (s, 1H). MS [(−)-ESI] m/z 428 [M − H]$^-$. Anal. ($C_{18}H_{13}Cl_2N_7O_2\cdot 0.5\ H_2O$) C, H, N.

3-(5-Amino-7-hydroxy-[1,2,3]triazolo[4,5-*d*]pyrimidin-2-yl)-*N*-benzo[1,3]dioxol-5-ylmethylbenzamide (28): ^{1}H NMR (300 MHz, DMSO-d_6) δ ppm 4.41 (d, J = 5.9 Hz, 1H), 5.98 (s, 2H), 6.73 (br s, 2H), 6.81−6.92 (m, 3H), 6.97−7.01 (m, 1H), 7.35−7.40 (m, 1H), 7.69 (t, J = 7.9 Hz, 1H), 7.97 (d, J = 7.7 Hz, 1H), 8.23 (dd, J = 7.7, 1.8 Hz, 1H), 8.59 (t, J = 1.8 Hz, 1H), 9.29 (t, J = 5.9 Hz, 1H), 11.05 (br s, 1H). MS [(−)-ESI] m/z 404 [M − H]$^-$.

3-(5-Amino-7-hydroxy-[1,2,3]triazolo[4,5-*d*]pyrimidin-2-yl)-*N*-[2-(2-hydroxymethylphenylsulfanyl)benzyl]-benzamide (29): ^{1}H NMR (300 MHz, DMSO-d_6) δ ppm 4.59 (t, J = 6.4 Hz, 4H), 5.33 (t, J = 5.5 Hz, 1H), 6.73 (br s, 2H), 7.06−7.15 (m, 2H), 7.21−7.29 (m, 2H), 7.31−7.41 (m, 3H), 7.57 (d, J = 7.4 Hz, 1H), 7.71 (t, J = 8.1 Hz, 1H), 8.00 (d, J = 8.1 Hz, 1H), 8.25 (dd, J = 8.8, 1.5 Hz, 1H), 8.63 (s, 1H), 9.32 (t, J = 5.7 Hz, 1H), 11.13 (m, 1 H). MS [(−)-ESI] m/z 498 [M − H]$^-$. Anal. ($C_{25}H_{21}N_7O_3\cdot 0.5\ H_2O$) C, H, N.

3-(5-Amino-7-hydroxy-[1,2,3]triazolo[4,5-*d*]pyrimidin-2-yl)-*N*-(2,3-dihydrobenzofuran-5-ylmethyl)benzamide (30): ^{1}H NMR (300 MHz, DMSO-d_6) δ ppm 3.15 (t, J = 8.7 Hz, 2H), 4.41 (d, J = 6.1 Hz, 2H), 4.49 (t, J = 8.8 Hz, 2H), 5.40 (s, 2H), 6.70 (d, J = 8.1 Hz, 1H), 7.07 (dd, J = 8.1, 2.0 Hz, 1H), 7.22 (s, 1H), 7.61 (t, J = 8.0 Hz, 1H), 7.83 (ddd, J = 7.9, 1.3, 1.0 Hz, 1H), 8.15 (ddd, J = 8.1, 2.4, 1.0 Hz, 1H), 8.53 (t, J = 1.9 Hz, 1H), 9.22 (t, J = 5.8 Hz, 1H). MS [(+)-ESI] m/z 402 [M − H]$^-$. Anal. ($C_{20}H_{17}N_7O_3\cdot H_2O$) C, H, N.

3-(5-Amino-7-hydroxy-[1,2,3]triazolo[4,5-*d*]pyrimidin-2-yl)-*N*-(3-hydroxypropyl)benzamide (31): ^{1}H NMR (500 MHz, DMSO-d_6) δ ppm 1.66 (m, 2H), 3.30 (t, J = 6.1 Hz, 2H), 3.37−3.46 (m, 3H), 6.68 (br s, 2H), 7.63 (t, J = 8.2 Hz, 1H), 7.89 (d, J = 7.9 Hz, 1H), 8.17 (d, J = 7.9 Hz, 1H), 8.50 (s, 1H), 8.69 (t, J = 5.5 Hz, 1H). MS [(−)-ESI] m/z 328 [M − H]$^-$.

3-(5-Amino-7-hydroxy-[1,2,3]triazolo[4,5-*d*]pyrimidin-2-yl)-*N*-(4-hydroxybutyl)benzamide (32): ^{1}H NMR (300 MHz, DMSO-d_6) δ ppm 1.43−1.63 (m, 4H), 3.40−3.50 (m, 4H), 4.40 (t, J = 5.2 Hz, 1H), 6.74 (br s, 2H), 7.68 (t, J = 7.9 Hz, 1H), 7.93 (d, J = 8.1 Hz, 1H), 8.21 (dd, J = 7.7, 1.8 Hz, 1H), 8.55 (t, J = 1.8 Hz, 1H), 8.77 (t, J = 5.5 Hz, 1H), 11.19 (br s, 1H). MS [(−)-ESI] m/z 342 [M − H]$^-$.

3-(5-Amino-7-hydroxy-[1,2,3]triazolo[4,5-*d*]pyrimidin-2-yl)-*N*-(2,2-bis-hydroxymethylbutyl)benzamide (33): ^{1}H NMR (300 MHz, DMSO-d_6) δ ppm 0.85 (t, J = 7.5 Hz, 3H), 1.29 (q, J = 7.5 Hz, 2H), 3.25−3.33 (m, 6H), 4.50 (t, J = 5.5 Hz, 2H), 6.70 (br s, 2H), 7.69 (m, 1H), 7.90 (d, J = 7.7 Hz, 1H), 8.24 (d, J = 7.7 Hz, 1H), 8.51 (s, 1H), 8.61 (t, J = 5.7 Hz, 1H), 10.51 (br s, 1H). MS [(−)-ESI] m/z 386 [M − H]$^-$.

3-(5-Amino-7-hydroxy-[1,2,3]triazolo[4,5-*d*]pyrimidin-2-yl)-*N*-(3-hydroxy-2,2-dimethylpropyl)benzamide (34): ^{1}H NMR (300 MHz, DMSO-d_6) δ ppm 0.86 (s, 6H), 3.16 (d, J = 6.1 Hz, 2H), 3.21 (d, J = 6.1 Hz, 2H), 4.59 (t, J = 5.8 Hz, 1H), 6.72 (br s, 2H), 7.70 (t, J = 8.0 Hz, 1H), 7.94 (ddd, J = 8.0, 1.4, 1.2 Hz, 1H), 8.23 (ddd, J = 8.2, 2.1, 0.85 Hz, 1H), 8.54 (t, J = 1.9 Hz, 1H), 8.67 (t, J = 6.3 Hz, 1H), 11.13 (s, 1H). MS [(−)-ESI] m/z 356 [M − H]$^-$. Anal. ($C_{16}H_{19}N_7O_3\cdot 0.5\ H_2O$) C, H, N.

3-(5-Amino-7-hydroxy-[1,2,3]triazolo[4,5-*d*]pyrimidin-2-yl)-*N*-(1-hydroxycyclohexylmethyl)benzamide (35): ^{1}H NMR (300 MHz, DMSO-d_6) δ ppm 1.17−1.62 (m, 10H), 3.20−3.30 (m, 2H), 4.38 (s, 1H), 6.75 (br s, 2H), 7.69 (t, J = 8.0 Hz, 1H), 7.97 (d, J = 7.8 Hz, 1H), 8.22 (dd, J = 8.1, 1.4 Hz, 1H), 8.50 (t, J = 5.6 Hz, 1H), 8.56 (s, 1H), 9.59 (br s, 1H). MS [(+)-ESI] m/z 384 [M + H]$^+$. Anal. ($C_{18}H_{21}N_7O_3\cdot 1.5\ H_2O$) C, H, N.

3-(5-Amino-7-hydroxy-[1,2,3]triazolo[4,5-*d*]pyrimidin-2-yl)-*N*-*cis*-(2-hydroxycyclohexylmethyl)benzamide (36): ^{1}H NMR (300 MHz, DMSO-d_6) δ ppm 1.20−1.25 (m, 1H), 1.28−1.40 (m, 4H), 1.52−1.74 (m, 4H), 3.15−3.25 (m, 2H), 3.78 (br s, 1H), 4.35 (d, J = 4.1 Hz, 1H), 6.72 (br s, 2H), 7.69 (t, J = 8.0 Hz, 1H), 7.94 (ddd, J = 8.1, 1.4, 1.0 Hz, 1H), 8.22 (ddd, J = 8.1, 2.4, 1.0 Hz, 1H), 8.54 (t, J = 1.9 Hz, 1H), 8.71 (t, J = 5.8 Hz, 1H), 11.11 (br s, 1H). MS [(−)-ESI] m/z 382 [M − H]$^-$. Anal. ($C_{18}H_{21}N_7O_3\cdot H_2O$) C, H, N.

3-(5-Amino-7-hydroxy-[1,2,3]triazolo[4,5-*d*]pyrimidin-2-yl)-*N*-trans-(2-hydroxycyclohexylmethyl)benzamide (37): ^{1}H NMR (300 MHz, DMSO-d_6) δ ppm 0.91−1.22 (m, 4H), 1.40−1.87 (m, 5H), 3.10−3.19 (m, 1H), 3.23−3.34 (m, 1H), 3.53 (td, J = 8.8, 4.8 Hz, 1H), 4.72 (d, J = 5.1 Hz, 1H), 6.72 (br s, 2H), 7.69 (t, J = 8.0 Hz, 1H), 7.94 (ddd, J = 8.0, 1.2, 1.0 Hz, 1H), 8.22 (ddd, J = 8.1, 2.2, 0.85 Hz, 1H), 8.54 (t, J = 1.9 Hz, 1H), 8.67 (dd, J = 6.1, 5.4 Hz, 1H), 11.12 (s, 1H). MS [(−)-ESI] m/z 382 [M − H]$^-$. Anal. ($C_{18}H_{21}N_7O_3\cdot H_2O$) C, H, N.

3-(5-Amino-7-hydroxy-[1,2,3]triazolo[4,5-*d*]pyrimidin-2-yl)-*N*-cis-(2-hydroxycycloheptylmethyl)benzamide (38): ^{1}H NMR (300 MHz, DMSO-d_6) δ ppm 1.32−1.83 (m, 11H), 3.19−3.37 (m, 2H), 3.86 (br s, 1H), 4.37 (d, J = 4.4 Hz, 1H), 6.73 (br s, 2H), 7.69 (t, J = 8.0 Hz, 1H), 7.94 (ddd, J = 8.0, 1.4, 1.2 Hz, 1H), 8.23 (ddd, J = 8.1, 2.0, 1.0 Hz, 1H), 8.55 (t, J = 1.9 Hz, 1H), 8.72 (t, J = 5.8 Hz, 1H), 11.13 (s, 1H). MS [(+)-DCI] m/z 398 [M + H]$^+$. Anal. ($C_{19}H_{23}N_7O_3\cdot H_2O$) C, H, N.

Supporting Information Available: ^{1}H NMR spectra for compounds **19**, **21**, **22**, and **24**−**38**. X-ray parameters and Protein Data Bank file names for DHNA/inhibitor complexes of compounds **11**−**15**, **19**, **27**, and **29**. This material is available free of charge via the Internet at http://pubs.acs.org.

References

(1) Chopra, I.; Hesse, L.; O'Neill, A. J. Exploiting current understanding of antibiotic action for discovery of new drugs. *Soc. Appl. Microbiol. Symp. Ser.* **2002**, *31*, 4S−15S. Daw, M. A.; Drah, A. M. Antibiotic resistance: Prospects for the new millennium. *J. Chemother.* **2001**, *13*, 587−594. Bax, R.; Mullan, N.; Verhoef, J. The millennium bugs—the need for and development of new antibacterials. *Int. J. Antimicrob. Agents* **2000**, *16*, 51−59. Domagala, J. M.; Sanchez, J. P. New approaches and agents to overcome bacterial resistance. *Annu. Rep. Med. Chem.* **1997**, *32*, 111−120.

(2) Lerner, C. G.; Beutel, B. A. Antibacterial drug discovery in the post-genomics era. *Curr. Drug Targets: Infect. Disord.* **2002**, *2*, 109−119. Chan, P. F.; Macarron, R.; Payne, D. J.; Zalacain, M.; Holmes, D. J. Novel antibacterials: a genomics approach to drug discovery. *Curr. Drug Targets: Infect. Disord.* **2002**, *2*, 291−308. Volker, C.; Brown, J. R. Bioinformatics and the discovery of novel anti-microbial targets. *Curr. Drug Targets: Infect. Disord.* **2002**, *2*, 279−290. Chalker, A. F.; Lunsford, R. D. Rational identification of new antibacterial drug targets that are essential for viability using a genomics-based approach. *Pharmacol. Ther.* **2002**, *95*, 1−20. Isaacson, R. E. Genomics and the prospects for the discovery of new targets for antibacterial and antifungal agents. *Curr. Pharm. Des.* **2002**, *8*, 1091−1098. McDevitt, D.;

Rosenberg, M. Exploiting genomics to discover new antibiotics. *Trends Microbiol.* **2001**, *9*, 611−617. Payne, D. J.; Holmes, D. J.; Rosenberg, M. Delivering novel targets and antibiotics from genomics. *Curr. Opin. Invest. Drugs* **2001**, *2*, 1028−1034. Holmes, D. J.; Throup, J. P.; Wallis, N. G.; Burnham, M. K. R.; Zalacain, M.; Biswas, S.; Chalker, A. F.; Ingraham, K. A.; Marra, A.; Bryant, A.; Woodnutt, G.; Warren, P. V.; Brown, J. R.; Rosenberg, M. The contribution of genomics to the discovery of new antibiotics. *Focus Biotechnol.* **2001**, *1*, 23−31. Lehoux, D. E.; Levesque, R. C. Detection of genes essential in specific niches by signature-tagged mutagenesis. *Curr. Opin. Biotechnol.* **2000**, *11*, 434−439. Reich, K. A. The search for essential genes. *Res. Microbiol.* **2000**, *151*, 319−324. Gray, C. P.; Keck, W. Bacterial targets and antibiotics. Genome-based drug discovery. *Cell. Mol. Life Sci.* **1999**, *56*, 779−787. Chopra, I. Prospects for antisense agents in the therapy of bacterial infections. *Expert Opin. Invest. Drugs* **1999**, *8*, 1203−1208. Kolstoe, A.-B. Dynamic bacterial genome organization. *Mol. Microbiol.* **1997**, *24*, 241−248. Miklos, G. L. G.; Rubin, G. M. The role of the genome project in determining gene function: insights from model organisms. *Cell* **1996**, *86*, 521−529.

(3) Bermingham, A.; Derrick, J. P. The folic acid biosynthesis pathway in bacteria: Evaluation of potential for antibacterial drug discovery. *BioEssays* **2002**, *24*, 637−648. Miller, G. H.; Doukas, P. H.; Seydel, J. K. Sulfonamide structure−activity relation in a cell-free system. Correlation of inhibition of folate synthesis with antibacterial activity and physicochemical parameters. *J. Med. Chem.* **1972**, *15*, 700−706. Hitchings, G. H. Folate antagonists as antibacterial and antiprotozoal agents. *Ann. N. Y. Acad. Sci.* **1971**, *186*, 444−451. Hitchings, G. H. Inhibitors of dihydrofolic acid reductase in the therapy of infectious diseases. *Bibl. Nutr. Diet.* **1966**, *8*, 226−237.

(4) Brown, G. M. Biosynthesis of pterins. *Folates Pterins* **1985**, *2*, 115−154.

(5) McCullough, J. L.; Maren, T. H. Inhibition of dihydropteroate synthetase from *Escherichia coli* by sulfones ad sulfonamides. *Antimicrob. Agents Chemother.* **1973**, *3*, 665−669. Ho, R. I.; Corman, L.; Morse, S. A.; Schneider, H. Structure activity of sulfones and sulfonamides on dihydropteroate synthetase from Neisseria meningitidis. *Antimicrob. Agents Chemother.* **1975**, *7*, 758−763. Vinnicombe, H. G.; Derrick, J. P. Dihydropteroate synthase: an old drug target revisited. *Biochem. Soc. Trans.* **1999**, *27*, 53−58.

(6) Hitchings, G. H., Jr. Selective inhibitors of dihydrofolate reductase (Nobel report). *Angew. Chem.* **1989**, *101*, 903−909. Periti, P. Evolution of the bacterial dihydrofolate reductase inhibitors. *J. Antimicrob. Chemother.* **1995**, *36*, 887−890. Roth, B.; Burchall, J. J. Small molecule inhibitors of dihydrofolate reductase. *Methods Enzymol.* **1971**, *18*, 779−786. Hitchings, G. H.; Burchall, J. J.; Ferone, R. Comparative enzymology of dihydrofolate reductase and the design of chemotherapeutic agents. *Symp. Soc. Gen. Microbiol.* **1966**, *16*, 294−300.

(7) Mathis, J. B.; Brown, G. M. Biosynthesis of folic acid. XI. Purification and properties of hydroneopterin aldolase. *J. Biol. Chem.* **1970**, *245*, 3015−3025.

(8) Zimmerman, M.; Tolman, R. L.; Morman, H.; Graham, D. W.; Rogers, E. F. Inhibitors of folate biosynthesis. 1. Inhibition of dihydroneopterin aldolase by pteridine derivatives. *J. Med. Chem.* **1977**, *20*, 1213−1215.

(9) Hennig, M.; D'Arcy, A.; Hampele, I. C.; Page, M. G. P.; Oefner, C.; Dale, G. E. Crystal structure and reaction mechanism of 7,8-dihydroneopterin aldolase from Staphylococcus aureus. *Nat. Struct. Biol.* **1998**, *5*, 357−362.

(10) Nienaber, V. L.; Richardson, P. L.; Klighofer, V.; Bouska, J. J.; Giranda, V. L.; Greer, J. Discovering novel ligands for macromolecules using X-ray crystallographic screening. *Nat. Biotechnol.* **2000**, *18*, 1105−1108.

(11) Muchmore, S. W. Experiences with CCD detectors on a home X-ray source. *Acta Crystallogr., Sect. D: Biol. Crystallogr.* **1999**, *D55*, 1669−1671.

(12) Bode, W.; Schwager, P. Refined crystal structure of bovine.beta.-trypsin at 1.8.ANG. resolution. II. Crystallographic refinement, calcium binding site, benzamidine binding site, and active site at pH 7.0. *J. Mol. Biol.* **1975**, *98*, 693−717.

(13) Benson, F. R.; Hartzel, L. W.; Savell, W. L. v-Triazolo[d]-pyrimidines. I. 2-Aryl-5-amino-7-hydroxy derivatives. *J. Am. Chem. Soc.* **1950**, *72*, 1816−1818.

(14) Crich, D.; Hao, X. Generation and Cyclization of Acyl Radicals from Thiol Esters under Nonreducing, Tin-Free Conditions. *J. Org. Chem.* **1997**, *62*, 5982−5988.

(15) Herrington, M. B. Measurement of the uptake of radioactive para-aminobenzoic acid monitors folate biosynthesis in *Escherichia coli* K-12. *Anal. Biochem.* **1994**, *216*, 427−430.

(16) Quinlivan, E. P.; McPartlin, J.; Weir, D. G.; Scott, J. Mechanism of the antimicrobial drug trimethoprim revisited. *FASEB J.* **2000**, *14*, 2519−2524.

(17) Otwinowski, Z.; Minor, W. Processing of X-ray diffraction data collected in oscillation mode. *Methods Enzymol.* **1997**, *276*, 307−326.

(18) Muchmore, S. W.; Olson, J.; Jones, R.; Pan, J.; Blum, M.; Greer, J.; Merrick, S. M.; Magdalinos, P.; Nienaber, V. L. Automated Crystal Mounting and Data Collection for Protein Crystallography. *Structure* **2000**, *8*, R243−R246.

(19) Harlan, J. Manuscript in preparation.

JM030497Y